Int. J. Heat Mass Transfer. Vol. 26, No. 9, pp. 1389–1401, 1983
Printed in Great Britain

0017-9310/83 $3.00 + 0.00

AN AXISYMMETRIC MODEL FOR THE CHARGING OF A LIQUID-DOMINATED GEOTHERMAL RESERVOIR

J. TRONCOSO and D. R. KASSOY
Department of Mechanical Engineering, University of Colorado, Boulder, CO 80309, U.S.A.

(*Received* 16 *March* 1982 *and in revised form* 13 *January* 1983)

Abstract—Heat and mass transfer processes occurring in a model of an axisymmetric liquid-dominated geothermal reservoir are described. The system is composed of a vertical cylindrical region of fractured rock surrounded by a much larger annular aquifer. Hot liquid water, convected into and up the central cylindrical zone is forced into the neighbouring aquifer. Heat is lost to the cold surface as the liquid flows horizontally (radially) in the aquifer. A combination of boundary layer techniques and numerical methods are used to obtain solutions for velocity, temperature and pressure distributions in the system and for the heat flux emanating from the surface of the cap rock. The deep portion of the axisymmetric aquifer is found to be cooled faster than the equivalent part of a planar model.

NOMENCLATURE

C_p	specific heat (of liquid) at constant pressure
g	gravity constant
k	permeability
l	clay cap thickness
L	aquifer depth
M	input mass flux
$O(\ )$	order symbol
P	liquid pressure
P_R	reference convection pressure
q_R	reference convection volumetric flow rate
r	radial coordinate
R	Rayleigh number
T	temperature
v	horizontal volumetric flow rate in the aquifer
V	horizontal volumetric flow rate in the fracture zone
W	vertical volumetric flow rate in the fracture zone
z	vertical coordinate

Greek symbols

α	thermal expansion coefficient of the liquid
λ	thermal conductivity
μ	dynamic viscosity of liquid
ν	kinematic viscosity of liquid
ρ	density of liquid
θ	temperature in the aquifer
τ	the overheat ratio, $(T'_{max} - T'_0)/T'_0$

Subscripts

ac	aquifer–clay cap interface
e	edge of fractured rock zone
F	fracture-zone value
h	horizontal (permeability)
H	hydrostatic value (with respect to ρ'_0)
m	mixture (porous material–liquid) value
max	reference values at bottom surface condition
0	reference values at upper surface condition
r	radial derivative
v	vertical (permeability)
z	vertical derivative

Superscripts

$(\ )'$	dimensional quantity
c	clay cap

1. INTRODUCTION

IT IS now widely acknowledged that fault zones play a significant role in the siting of liquid-dominated geothermal reservoirs [1–22]. In general, the fracture systems associated with faulting provide the vertical permeability necessary for liquid water, heated at depth, to be convected upward into shallow permeable sediments. This fault-zone controlled charging process can lead to the formation of a geothermal reservoir relatively close to the surface. Extensive discussion of the conceptual notions involved can be found in the references cited above.

Heat and mass transfer processes in models of fault zones have received considerable attention. For example Murphy [9], Lowell and Shyu [23] and Lowell [10, 24] have examined the characteristics of convection processes in models of fault zones with impermeable, heat conducting vertical boundaries. The studies are formulated in terms of a finite dimension, thin vertical slab of porous medium, saturated with water, which is heated at the impermeable lower horizontal surface and cooled at the upper impermeable boundary. The mass flux is entirely internal to this model of a confined fault zone.

Sorey [11] and Nathenson *et al.* [12] have examined the temperature distributions in impermeable rocks adjacent to a fault zone through which there is a prescribed mass flow of initially hot liquid. The liquid cools as it rises in the fault and exits at the surface. Kassoy and Zebib [13] examined the fluid mechanics of a heated liquid stream passing through a vertical fault zone toward the surface. The vertical boundaries of the fault are impermeable. Conditions for 2- and 3-dimensional convection configurations are discussed.

Convection processes in confined fault zones, with open, upper, cool boundaries, have been discussed by Turcotte *et al.* [14] and Lowell [24]. Results are given for the mass flux and temperature of the fluid exiting at the surface in the upflow region.

One may contrast the heat and mass transfer studies in the fault zones with impermeable vertical boundaries to those which emphasize the charging of permeable aquifers adjacent to the fault zones containing upflow of liquid heated at depth. Pritchett and Garg [15] provide a simple model of this process where the fault is treated as a source of hot liquid. Applications to elementary models of geothermal aquifers have been given [16–18].

A planar model of fault-zone controlled charging of a geothermal reservoir has been developed by Goyal [2] and Goyal and Kassoy [1, 3], motivated by field data obtained primarily from the East Mesa system [25]. This fault is modelled as a thin vertical slab of porous medium with isotropic permeability. The neighbouring sediments, dominated by a shaly stratigraphy which minimizes vertical motion, are represented by a porous medium with horizontal permeability only. In the more realistic of the models, the surface sediments are modelled by an entirely impermeable layer of material in which conduction is the sole means of energy transfer. Liquid water, heated at depth, moves upward in the vertical slab and then spreads laterally, in an isothermal manner, into the nearby sections of the aquifer. Initially, the cooling effect of the upper surface on the aquifer fluid is confined to a thin layer adjacent to the cap–reservoir interface near the fault. This boundary layer grows with distance from the fault. Eventually the entire depth of the aquifer is cooled by heat loss to the surface. Boundary layer theory and numerical methods are used to obtain solutions for the distribution of velocity, temperature and pressure within the system and for the heat flux at the upper surface. The capped model described in ref. [3] is shown to be representative of the processes occurring at the Mesa system. Some of the quantitative discrepancies between the field data and the model-based predictions can be attributed to the local geometry of the system where the most vigorous geothermal activity is found. In particular, the surface heat flux patterns shown in Figs. 2 and 13 of ref. [3] suggest that the system is more axisymmetric than planar in the local region where the flux is maximized.

Riney *et al.* [4, 5, 26, 27] have developed a 3-dim. conceptual model of the East Mesa system which is reminiscent of that described in refs. [1–3]. The mathematical model is derived from the equations for flow in saturated porous media. Solution development is based on several numerical codes (MUSHRM and LIGHTS). These codes include far more general rock and water material properties than those employed in the quasi-analytical studies of refs. [1–3]. The permeability is generally anisotropic and inhomogeneous. A specifically axisymmetric model is described in refs. [4, 5, 26]. A vertical section of the reservoir from the axis to the prescribed radius of the outer boundary is divided into a variably spaced finite-difference grid with 5 cells in the vertical direction and 13 in the radial direction. Each cell can be identified with distinct material properties which are obtained from field data analysis. The entry of hot liquid into the bottom of the system is modelled by a mass source in the deepest cell adjacent to the axis. The prescribed temperature on the lower boundary decreases gradually with radial distance from the axis. In effect the upper boundary is held at a fixed surface temperature, although the details of the heat loss process through the upper cap layer are reduced to a heat sink expression derived from a heat transfer coefficient relationship. At the outer radial location the temperature variation with depth is assumed to be controlled purely by conduction. The resulting pressure distribution is hydrostatic.

Successful calculations were performed with horizontal permeabilities, k'_h, between 2×10^{-14} and 9×10^{-14} m^2 in the fluid dynamically active layers of the reservoir and a vertical permeability, k'_v of about 5×10^{-16} m^2. The very low prescribed vertical permeability in every cell implies that the model does not contain an explicit highly localized vertical zone of significant vertical permeability (the result of fault-zone fracturing) through which fluid can rise from depth.

In the present work we extend our earlier studies of planar systems to describe a generic model of axisymmetric aquifer charging resulting from upflow in an explicit localized region of high vertical permeability. The latter can be thought of as resulting from the intersection of several linear fault zones, each of which contains extensively fractured material. The intersection region can be modelled as a cylinder of porous medium with isotropic permeability. Surrounding the cylinder is a far larger annulus of porous material representing the aquifer, which is characterized by a finite horizontal permeability and zero vertical permeability. The latter condition is used to preclude large scale vertical motion which, in the field is suppressed by extensive interbedding of shales and sands [1–3, 7, 25]. The entire system is covered by an impermeable cap layer. The mass flux into the fractured central zone is prescribed. A combination of boundary layer methods and numerical techniques are used to obtain solutions for the temperature, pressure and velocity in the system and for the surface heat flux distribution. At a given depth in the aquifer we find that the temperature decline with distance from the axis is considerably faster than that found in the planar model. The decrease of the radial fluid velocity with increasing radius, reduces the effectiveness of convective transport of hot liquid from the fracture zone thus permitting relatively rapid cooling of the aquifer by vertical conduction to the cold surface.

2. CONCEPTUAL MODEL

The conceptual model of the region studied is shown in Fig. 1. The intersection region is conceptualized as a

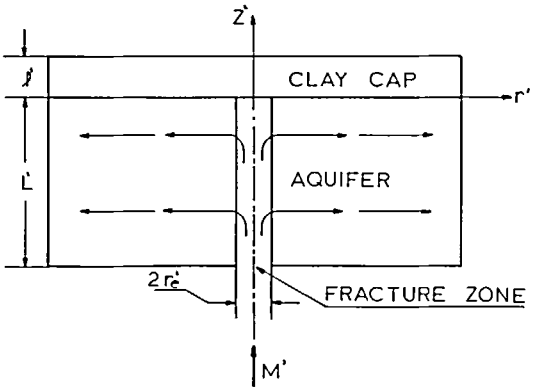

FIG. 1. A vertical section of the axisymmetric system showing structural components and dimensions.

vertical cylinder of radius r'_c and height L' of highly permeable material, which extends from the bottom of the clay cap downward through the basement rock. An impermeable clay-rich cap of thickness l' overlies the axisymmetric aquifer. The permeability of the aquifer in the horizontal direction is much greater than in the vertical direction. This difference is due to the observed shaly layers associated with interbedding.

Water heated at depth, presumably in a fractured basement rock, rises in the permeable cylindrical fracture zone associated with the fault intersections. The vertical speed of the water is sufficiently large to ensure that convective heat transport overwhelms heat transfer associated with conduction. Vertical motion is suppressed at the top of the fault by the presence of the impermeable clay-rich cap. The horizontal pressure gradient associated with convection forces the water into the neighbouring horizontal layers of porous rock (aquifer). Initial cooling of the aquifer occurs in a thin layer just below the aquifer–cap boundary in the neighbourhood of the cylinder. At sufficiently large distances from the cylinder boundary the entire aquifer is cooled. The vertical heat transfer process in the aquifer is by conduction alone because the water moves only in the horizontal direction. Horizontal heat transport is primarily convective in nature. Heat removed from the aquifer is conducted through the clay cap and lost at the surface.

The original motivation for studying a cylindrical charging model arose from the observation of non planar local effects in the most vigorous part of the East Mesa system [3]. It was recognized that the decline of flow rate with increasing radial distance would have a profound effect on the aquifer heat transfer process. From the viewpoint of modelling, the present study represents an attempt to quantify the geometric effect rather than to model the East Mesa system in particular.

3. MATHEMATICAL MODEL

The fracture zone is modelled as a vertical cylinder of porous medium with equal horizontal and vertical permeability for simplicity. In the cylindrically axisymmetric aquifer it is assumed that vertical permeability is absent. This condition is imposed in order to model the effects of extensive interbedding of shales and sands, which in effect shut off large scale vertical motion [1–3]. The horizontal permeability is assumed to be the same as that in the fracture zone for mathematical convenience.

Spatially uniform temperatures are imposed on the bottom boundary and on the top of the clay cap of the reservoir. As a result, far from the upflow fracture zone, the horizontal temperature gradient must vanish everywhere in the cap and aquifer. It follows then that the heat transfer far from the upflow zone is purely by vertical conduction.

A complete derivation of the equations for a liquid saturated porous medium are given by Goyal [2]. The describing steady dimensional equations for the axisymmetric system in cylindrical coordinates are given by

Fracture zone.

$$\frac{1}{r'}(r'V')_{r'} + W'_{z'} = 0, \tag{1}$$

$$\frac{\mu'}{k'}V' = -P'_{\mathrm{F},r'}. \tag{2}$$

$$\frac{\mu'}{k'}W' = -(P'_{\mathrm{F}} - P'_{\mathrm{H}})_{z'} + g(\rho' - \rho'_0), \tag{3}$$

$$C'_p(V'T'_{r'} + W'T'_{z'}) = \lambda'_{\mathrm{m}}\left(\frac{1}{r'}(r'T'_{r'})_{r'} + T'_{z'z'}\right), \tag{4}$$

$$\rho' = \rho'_0[1 - \alpha'(T' - T'_0)]. \tag{5}$$

Aquifer.

$$(r'v')_{r'} = 0, \tag{6}$$

$$\frac{\mu'}{k'}v' = -P'_{r'}, \tag{7}$$

$$C'_p v'\theta'_{r'} = \lambda'_{\mathrm{m}}\left[\frac{1}{r'}(r'\theta'_{r'})_{r'} + \theta'_{z'z'}\right]. \tag{8}$$

Clay cap.

$$\lambda'^{c}_{\mathrm{m}}\left[\frac{1}{r'}(r'T'^{c}_{r'})_{r'} + T'^{c}_{z'z'}\right] = 0. \tag{9}$$

The previous equations are obtained assuming that the flow is steady, the solid matrix is rigid, the fracture zone medium is isotropic and homogeneous, the liquid properties (except density) are assumed to be constant, the conductivity of the fracture zone and aquifer are equal and constant, the clay cap is impermeable, the permeability of the fracture zone is equal to the horizontal value in the aquifer and the vertical permeability of the aquifer is zero. In addition the Boussinesq approximation is applied.

The system of equations (1)–(9) is subjected to the following boundary and continuity conditions:

3.1. *Boundary conditions*

Fracture zone.

$$W'(r', 0) = 0, \quad \text{(impermeability of the clay cap)} \tag{10}$$

$$2\pi \int_0^{r'_e} \rho' W'(r', -L') r' \, dr' = M', \quad \text{(input mass flow rate)} \tag{11}$$

$$T'(r', -L') = T'_{max}, \text{(hot lower boundary)} \tag{12}$$

$$T'_{r'}(0, z') = 0. \text{ (symmetry)} \tag{13}$$

Aquifer.

$$\theta'(r', -L') = T'_{max}, \text{(hot lower boundary)} \tag{14}$$

$$\theta'(r' \to \infty, z') = T'_{ac} - (T'_{max} - T'_{ac}) \times (z'/L'), \quad -L' \leqslant z' \leqslant 0. \tag{15}$$

Clay cap.

$$T^{c'}(r', l') = T'_0, \text{(cold upper boundary)} \tag{16}$$

$$T^{c'}(r' \to \infty, z') = T'_{ac} - (T'_{ac} - T'_0) \times (z'/l'), \quad 0 \leqslant z' \leqslant l', \tag{17}$$

$$T^{c'}_{r'}(0, z') = 0 \text{ (symmetry)}$$

where T'_{ac}, the aquifer clay cap interface temperature far from the fracture zone, can be expressed as

$$T'_{ac} = \frac{\lambda'_m l' T'_{max} + \lambda^{c'}_m L' T'_0}{l' \lambda'_m + L' \lambda^{c'}_m}. \tag{18}$$

3.2. *Continuity conditions*

Fracture zone–aquifer boundary.

$$T'(r'_e, z') = \theta'(r'_e, z'), \tag{19}$$

$$V'(r'_e, z') = v'(r'_e, z'), \tag{20}$$

$$P'_F(r'_e, z') = P'(r'_e, z'). \tag{21}$$

Fracture zone–clay cap boundary.

$$T'(r', 0) = T^{c'}(r', 0), \tag{22}$$

$$\lambda'_m T'_{z'}(r', 0) = \lambda^{c'}_m T^{c'}_{z'}(r', 0). \tag{23}$$

Aquifer–clay cap boundary.

$$\theta'(r', 0) = T^{c}(r', 0), \tag{24}$$

$$\lambda'_m \theta'_{z'}(r', 0) = \lambda^{c'}_m T^{c'}_{z'}(r', 0). \tag{25}$$

4. NON-DIMENSIONAL EQUATIONS

Non-dimensional equations describing the flow field can be developed in terms of the variables

$$v = \frac{v'}{q'_R}, \quad V = \frac{V'}{q'_R}, \quad \bar{r} = \frac{r'}{L'}, \quad z = \frac{z'}{L'},$$

$$\rho = \frac{\rho'}{\rho'_0}, \quad T = \frac{T'}{T'_0}, \quad T^c = \frac{T^{c'}}{T'_0}, \quad \theta = \frac{\theta'}{T'_0},$$

$$P_F = \frac{P'_F - P'_H}{P'_R}, \quad P = \frac{P' - P'_H}{P'_R}, \quad W = \frac{W'}{q'_R}, \tag{26}$$

where

$$\lambda = \frac{\lambda^{c'}_m}{\lambda'_m}, \quad l = \frac{l'}{L'}, \quad r_e = \frac{r'_e}{L'},$$

and

$$q'_R = \frac{g' k' \alpha' (T'_{max} - T'_0)}{\nu'} \text{: reference convection velocity,} \tag{27}$$

$$P'_R = \rho'_0 g' \alpha' L' (T'_{max} - T'_0) \text{:}$$

reference convection pressure. (28)

The non-dimensional Rayleigh number is defined as

$$R = \frac{\rho'_0 q'_R C'_p (T'_{max} - T'_0)}{\lambda'_m \left(\dfrac{T'_{max} - T'_0}{L'} \right)} \gg 1. \tag{29}$$

Far from the fracture zone ($r' \to \infty$) the temperature, controlled primarily by conduction, is expressed as

$$T^{c'} = T'_0 + \frac{(T'_{max} - T'_0)}{(\lambda^{c'}_m/\lambda'_m + l'/L')} \left(\frac{l' - z'}{L'} \right), \quad 0 \leqslant z' \leqslant l' \tag{30}$$

in the cap, and as

$$\theta' = T'_0 + \frac{(T'_{max} - T_0)}{(\lambda^{c'}_m/\lambda'_m + l'/L')} \left[\frac{l' - z'(\lambda^{c'}_m/\lambda'_m)}{L'} \right], \quad -L' \leqslant z' \leqslant 0 \tag{31}$$

in the aquifer.

The corresponding hydrostatic pressure field in the aquifer is written as

$$P'_H = P'_0 + \rho'_0 g' (l' - z') - \frac{P'_R}{2L'^2} \times \left[\frac{l'^2 + (\lambda^{c'}_m/\lambda'_m) z'^2 - 2l'z'}{(\lambda^{c'}_m/\lambda'_m + l'/L')} \right], \quad -L' \leqslant z' \leqslant 0. \tag{32}$$

The first two terms in equation (32) represent the hydrostatic head based on the cold surface density ρ'_0. The last term is a correction for the density variation with the temperature in equation (31).

The non-dimensional equations can be derived from equations (1)–(9) and equations (26)–(29). For example, in the fracture zone, where the appropriately scaled variables are

$$\bar{r} = r_e \hat{r}, \quad V = r_e \hat{V}, \tag{33}$$

we find

$$\frac{1}{\hat{r}} (\hat{r} \hat{V})_{\hat{r}} + W_z = 0, \tag{34}$$

$$r_e^2 \hat{V} = -P_{F,\hat{r}}, \tag{35}$$

$$W = -P_{F,z} + \frac{T - 1}{\tau}, \tag{36}$$

$$R r_e^2 (\hat{V} T_{\hat{r}} + W T_z) = \frac{1}{\hat{r}} (\hat{r} T_{\hat{r}})_{\hat{r}} + r_e^2 T_{zz}. \tag{37}$$

The equations describing the aquifer heat and mass

transfer can be written as

$$(\bar{r}v)_{\bar{r}} = 0, \tag{38}$$

$$v = -P_{\bar{r}}, \tag{39}$$

$$Rv\theta_{\bar{r}} = \frac{1}{\bar{r}}(\bar{r}\theta_{\bar{r}})_{\bar{r}} + \theta_{zz}. \tag{40}$$

Finally the conduction equation in the cap has the form

$$\lambda\left[\frac{1}{\bar{r}}(\bar{r}T^{c}_{\bar{r}})_{\bar{r}} + T^{c}_{zz}\right] = 0. \tag{41}$$

Far from the fracture zone, the aquifer temperature distribution is given by

$$\theta = 1 + \frac{\tau}{\lambda + l}(l - \lambda z), \quad -1 \leqslant z \leqslant 0 \tag{42}$$

and by

$$T^{c} = 1 + \frac{\tau}{\lambda + l}(l - z), \quad 0 \leqslant z \leqslant l \tag{43}$$

in the cap. The far field pressure is described by

$$P_{FF} = -\frac{l^2 + \lambda z^2 - 2lz}{2(\lambda + l)}, \quad -1 \leqslant z \leqslant 0. \tag{44}$$

5. SOLUTION DEVELOPMENT

The solutions are developed in terms of asymptotic expansions [28] valid in the limit of large Rayleigh number. In particular we consider $r_e \to 0$ for $Rr_e^2 = O(1)$. The analytical methods are similar in spirit to those used by Goyal [2] and Goyal and Kassoy [1, 3] for the planar problem. An explicit description of the analysis in cylindrical coordinates is presented in order to emphasize the effects of geometry on the results. The disinterested reader may proceed to the Discussion where the mathematical results are described in more physical terms.

The fracture-zone equations (34)–(37) are solved along with boundary and continuity conditions written in the form

$$W(\hat{r}, 0) = 0, \quad W(\hat{r}, -1) = M, \tag{45}$$

$$\hat{V}(\hat{r} = 1, z) = \hat{v}(\hat{r} = 1, z), \quad \hat{v} = v/r_e, \tag{46}$$

$$T(\hat{r}, -1) = 1 + \tau, \quad T_{\hat{r}}(0, z) = 0 \tag{47}$$

where

$$M = M'/M'_R, \quad M'_R = \rho'_0 q'_R \pi r'^2_e. \tag{48}$$

In equation (46), $\hat{v}(\hat{r}, z)$ represents the scaled horizontal speed in the aquifer in the region where $1 \leqslant \hat{r} = O(1)$.

In a high Rayleigh number flow, energy transfer associated with convection is far greater than that due to conduction. As a result fluid entering the fracture zone will flow vertically without significant change in temperature except in a thin boundary layer near the top of the fracture zone where heat transfer by conduction must play a role.

To lowest order, equation (37) is satisfied by

$$T_0 = 1 + \tau, \quad -1 \leqslant z \leqslant 0. \tag{49}$$

It follows from equations (34)–(36) and (49) that to a first approximation

$$W_0 = W_0(z), \quad \hat{V}_0 = -W_{0z}\frac{\hat{r}}{2} \tag{50}$$

and

$$P_{F0} = P_{F0}(z = -1) + 1 + z - \int_{-1}^{z} W_0(\sigma)\, d\sigma. \tag{51}$$

The function $W_0(z)$ remains to be found in the course of the analysis.

The solution must now be continued into the adjacent aquifer. The exact general solution to equations (38) and (39) can be written as

$$v = \frac{F(z, r_e)}{\bar{r}}, \quad P = A(z; r_e) - F(z; r_e)\ln \bar{r} \tag{52}$$

where lowest order approximations to A and F are found by invoking continuity of horizontal speed and pressure at $\hat{r} = 1$. It follows that

$$F_0 = r_e^2\frac{|W'_0(z)|}{2}, \quad A_0 = P_{F0}(z). \tag{53}$$

The logarithmic decline of the pressure field from the fault-zone value $P_{F0}(z)$ is associated with the inverse radial dependence of the horizontal speed. Of course the actual magnitude of the decline is small, $O(r_e^2)$, in the $\bar{r} = O(1)$ region.

In equation (40), the term $Rv = O(Rr_e^2) = O(1)$ when $\bar{r} = O(1)$, given the results in equations (52) and (53). It follows that there is a full balance between horizontal convection and conduction in that region of the aquifer scaled on the depth of the system. The $\theta(\bar{r}, z)$ solution is considered in a subsequent section.

Eventually the basic pressure distribution must make a transition to a value close to that in the far field, P_{FF}, given in equation (44). The nonuniformity in the pressure result in equations (52) when $\bar{r} \to \infty$ suggests the far-field scaling $\bar{r} = \alpha(r_e)\tilde{r}$, $\alpha = o(1)$ in the limit $r_e \to 0$. Then equations (52) and (53) can be used to show that

$$v = r_e^2\alpha(r_e)\frac{|W'_0|}{2\tilde{r}},$$

$$P(\tilde{r} \to 0, z) \sim P_{F0}(z) + r_e^2 \ln(\alpha)\frac{|W'_0|}{2} + o(1) \tag{54}$$

where the expression for P is a formal matching condition, while that for v is the exact solution. In order to find $\alpha(r_e)$ it is necessary to relate the exact solution for P in the $\tilde{r}$-region

$$P = \tilde{A}(z; r_e) - F(z; r_e)\ln \tilde{r} \tag{55}$$

found from equations (52) and the $\tilde{r}$-definition, with the matching condition. In equation (55), the basic pressure field is given by the first approximation to $\tilde{A}$ because

$F = O(r_e^2)$. Thus, lowest order matching requires that

$$\tilde{A}_0(z) = P_{F0}(z) + r_e^2 \ln(\alpha)\frac{|W_0'|}{2}. \quad (56)$$

Finally, in the $\tilde{r}$-region, the energy equations (40) and (41) reduce to the elementary forms $\theta_{zz} = O(\alpha^2)$, $T^c_{zz} = O(\alpha^2)$ in the limit $r_e \to 0$. Given the constant temperature boundary conditions on the upper and lower surfaces of the system, the lower order approximations to the solution are given precisely by the purely conductive distributions in equations (42) and (43). It follows that the associated basic pressure distribution is simply the far-field hydrostatic value; $\tilde{A}_0 = P_{FF}(z)$ given in equation (44). Then one can choose $\alpha = \exp(-2/r_e^2)$ so that

$$P_{FF}(z) = P_{F0}(z) - |W_0'|. \quad (57)$$

If equation (57) is differentiated once, one finds

$$W_0''(z) - W_0 = -\frac{\lambda}{(\lambda+l)}(1+z). \quad (58)$$

The solution satisfying equations (45) can be written as

$$W_0(z) = b[1+z-\cosh(z)] - a\sinh(z) \quad (59)$$

where

$$a = \frac{M + \dfrac{\lambda}{\lambda+l}\cosh(1)}{\sinh(1)} \quad \text{and} \quad b = \frac{\lambda}{\lambda+l}.$$

Then from equations (50) and (51) one can obtain the fracture-zone solutions for $\hat{V}_0$ and P_{F0}. The aquifer solutions in the $\hat{r}$- and $\bar{r}$-regions are given by equations (52) and (53). Finally the far-field velocity is given in equation (54) and the pressure solution by equations (55)–(59).

The logarithmic dependence of the exact pressure solution in equation (55) implies that the far-field conditions must really be applied at a finite but large value of r' rather than infinitely far away as suggested in equations (15) and (17). This was also the case in the planar problem [1,3]. In dimensional terms, the $\tilde{r}$-region is described by $r' = O[L' \exp(2/r_e^2)]$ which is typically enormous relative to the system depth. It is not surprising that the temperature field is basically (vertically) conductive so far from the upflow zone.

6. TEMPERATURE SOLUTIONS IN THE FRACTURE ZONE, AQUIFER AND CLAY CAP

Temperature distributions in the aquifer–fracture-zone–clay cap system have to be calculated in each of the regions shown in Fig. 2.

The energy equations in several essential regions are given in equations (60)–(63) in terms of appropriately scaled variables.

Region 1′

$$Rr_e^2(\hat{V}T_{\hat{r}} + \hat{W}T_{\hat{z}}) = \frac{1}{\hat{r}}(\hat{r}T_{\hat{r}})_{\hat{r}} + T_{\hat{z}\hat{z}}, \quad (60)$$

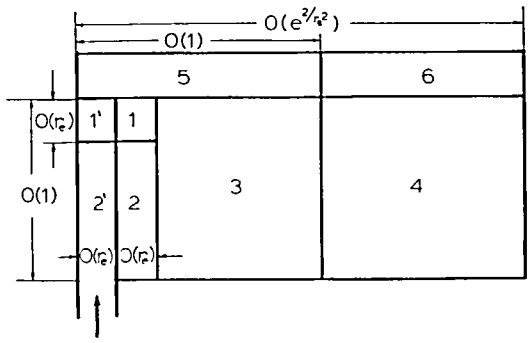

FIG. 2. System map indicating location of regions discussed in Section 6.

Region 2

$$r_e^2(Rr_e^2)\bar{v}\theta_{\bar{r}} = \frac{r_e^2}{\hat{r}}(\hat{r}\theta_{\hat{r}})_{\hat{r}} + \theta_{zz}, \quad (61)$$

Region 3

$$Rr_e^2\bar{v}\theta_{\bar{r}} = \frac{1}{\bar{r}}(\bar{r}\theta_{\bar{r}})_{\bar{r}} + \theta_{zz}, \quad (62)$$

Region 5

$$\lambda\left[\frac{1}{\bar{r}}(\bar{r}T^c_{\bar{r}})_{\bar{r}} + T^c_{zz}\right] = 0 \quad (63)$$

where

$$\hat{z} = \frac{z}{r_e} = \frac{z'}{r_e'}, \quad W = r_e\hat{W}, \quad V = r_e\hat{V}, \quad v = r_e^2\bar{v}.$$

6.1. *Solution in Regions 1′ and 5*

Liquid entering the system has a characteristic vertical speed q_R' which is large enough to ensure that $R \gg 1$. Then to a first approximation, the flow is isothermal ($T_0 = 1+\tau$) in Region 2′. In Region 1′, the fluid must lose heat by conduction to the cooler clay cap. Temperature solutions for equations (60) and (63), developed by Troncoso [6], can be written as

$$T = 1+\tau - r_e\frac{\lambda\tau\sqrt{\pi}}{2\gamma_1 l}[1+\operatorname{erfc}(\gamma_1\hat{z})] + O(r_e^2) \quad (65)$$

in the boundary layer and as

$$T^c = 1+\tau\left(1-\frac{z}{l}\right) - r_e\frac{\lambda\tau\sqrt{\pi}}{2\gamma_1 l} \times\left(1-\frac{z}{l}\right) + O(r_e^2), \hat{r} \leqslant 1 \quad (66)$$

in the cap, where

$$\gamma_1 = \left[\frac{Rr_e^2}{2}(a-b)\right]^{1/2}.$$

The $O(1)$ terms in equations (65) and (66) are valid for $0 \leqslant \hat{r} < \infty$. However, the smaller $O(r_e)$ terms are useful only in or above the fracture zone itself, $(0 \leqslant \hat{r} \leqslant 1)$. When $1 < \bar{r} \leqslant \infty$, the $O(r_e)$ solution structure for the clay cap (Region 5) and the aquifer (Region 1) is more

complex. From the viewpoint of obtaining basic approximations to the system these solutions are not essential to the analysis. They will not be considered further.

6.2. *Solution in Regions* 2, 4 *and* 6

The solutions in Regions 2, 4 and 6 are easy to obtain because the describing equations reduce to pure conduction forms in the limit $r_e \to 0$. For example, the boundary condition for equation (61) given in equation (47) implies that $\theta_0 = 1+\tau$. This means that the hot liquid originating from the fracture zone flows isothermally in the Region 2 aquifer. Far from the fracture zone where conduction heat transfer predominates, the results in equations (42) and (43) are the appropriate basic solutions as explained earlier.

6.3. *Solution in Regions* 3 *and* 5

In Region 3, there exists a balance between horizontal convective heat transfer and heat conduction in the limit $r_e \to 0$ when $Rr_e^2 = O(1)$. Temperatures in Region 3 and in the clay cap overlying it are obtained by integrating equations (62) and (63) numerically. In the former $\bar{v}$ is obtained from equations (52) and (64).

In order to ensure continuous temperature and heat flux at the clay cap–aquifer interface, the numerical solution utilized an integral energy balance approach in the neighbourhood of the interface. In a similar way an energy balance is carried out in the clay cap (Region 5) and in the aquifer (Region 3). The spatial gradients are represented by a finite difference method employing a five-point approximation of second order accuracy. An unequal mesh spacing is used in both the $\bar{r}$-radial and z-vertical directions. The radial dimension of the mesh-space increases in size from the fracture zone to the estimated far-field boundary. This solution obtained by numerical integration is only valid in the region where the radial distance from the fracture zone $\bar{r} = O(1)$ in the limit $r_e \to 0$. A complete formulation of the numerical procedure is given by Troncoso [6].

7. RESULTS

Representative parameter values for a liquid dominated hydrothermal system [2] are $R = 500$, $\tau = 1$, $\lambda = 0.7$, $r_e = 0.025$ and $l = 0.24$. Typical quantitative results will be based on these parameter values.

The vertical velocity distribution in the fracture zone given in equation (59) can be written in the form

$$W_0(z) = M\frac{\sinh|z|}{\sinh(1)} + \left[\frac{\lambda}{\lambda+l}\right]\left[1-|z|-\frac{\mathrm{sh}(1-|z|)}{\mathrm{sh}(1)}\right], \quad -1 \leqslant z \leqslant 0. \quad (67)$$

A pure convection effect is represented by the term linearly proportional to the mass input M. The second term, a modification associated with conductive heat transfer through the cap, is never more than 0.045 in magnitude relative to the $O(1)$-convection effect. Typical results are given in Fig. 3. The value W_0 increases with depth because the overpressure associated with convection pushes fluid into the aquifer. In Fig. 4, P_{F0} is shown as a function of depth for different mass flow rates. The pressure distribution from equation (57) is written as

$$P_{F0} = M\frac{\cosh(z)}{\sinh(1)} + \left[\frac{\lambda}{\lambda+l}\right] \times\left[\frac{\mathrm{ch}(1-|z|)}{\mathrm{sh}(1)}-1\right]-\frac{(l^2+2l|z|+\lambda z^2)}{2(\lambda+l)}. \quad (68)$$

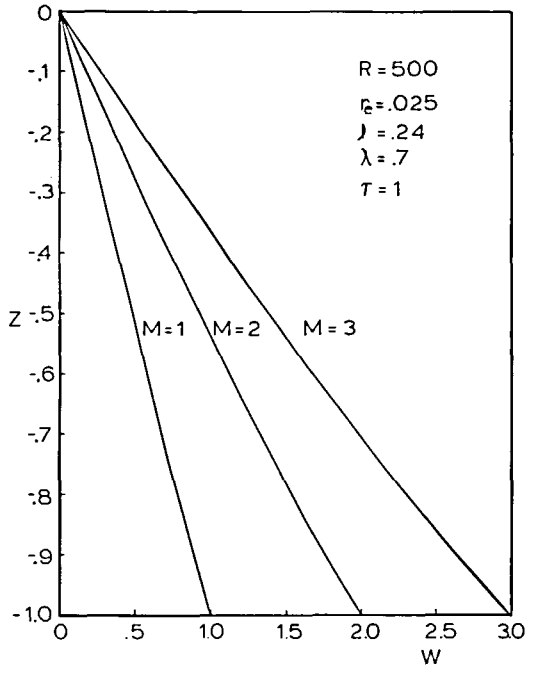

FIG. 3. Vertical velocity in the fracture zone as a function of depth for several mass flow rates.

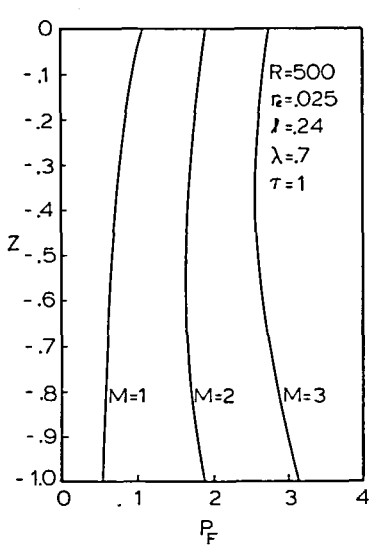

FIG. 4. Pressure in the fracture zone as a function of depth for several mass flow rates.

The first term represents the effect of mass input. Heat transfer through the cap produces the modification in the second term which is never larger than 0.115. The third term describes the difference between the hot and cold hydrostatic head. It should be noted from equation (26) that P_{F0} is the difference between the actual pressure and the cold hydrostatic head.

When $M = 1$, P_{F0} decreases monotonically with depth in the fracture zone. The maximum value occurs near the stagnation point at $z = 0$. When the mass flux is larger, the pressure distribution is somewhat different. Higher values of P_{F0} are observed deep in the system. It should be noted from equations (27) and (48) that $M = 1$ corresponds to an input mass flux associated with the characteristic vertical natural convection speed q'_R. This quantity is the equilibrium speed achieved by a material element of liquid water at a temperature T'_{max} moving purely as a result of buoyancy in a saturated porous medium at a temperature T'_0. {A force balance between the buoyant force $(\rho' - \rho'_0)g'$ and the medium resistance force $(\mu'/k')q'_R$, along with the equation of state $\rho' \simeq \rho'_0 [1 - \alpha'(T'_{max} - T'_0)]$, gives the desired result.} For parameter values typical of geothermal systems ($k' = 10^{-13}$ m^2, $\alpha' = 10^{-3}$ K^{-1}, $\nu' = 0.25 \times 10^{-6}$ m^2 s^{-1}, $\Delta T = 200$ K), $q'_R = O(10^{-4}$ cm s$^{-1})$. The associated characteristic mass flux $M'_R = O(10$ kg s$^{-1})$ for $r'_e = 80$ m ($r_e = 0.025$). When $M > 1$, the outlet mass flux is not determined strictly by the temperature difference $(T'_{max} - T'_0)$, the fracture-zone permeability k' and the water viscosity μ'. For example, artesian pressures associated with elevated terrain may enhance the buoyancy driven vertical speed. More conjecturally, if the feed system near the bottom of the central fracture zone is dominated by a few large cracks, then the characteristic input rate may be controlled by hydraulic processes not directly related to buoyancy-driven flow in a porous medium.

Figure 5 shows the variation of the horizontal aquifer velocity $\hat{v}$ with radius $\hat{r}$ for $z = -0.5$ and the parameter values noted. The result is obtained from equations (46), (52), and (53), where the z-dependent portion of the radial velocity is represented by the first two terms in equation (68). At $z = -1$ the velocity is about 1.5 times the value at $z = 0$, the aquifer–cap interface. In this sense a disproportionate amount of hot liquid tends to move through the deeper portions of the aquifer. In this region close to the fracture zone the typical dimensional horizontal speed is $O(10^{-8}$ m s$^{-1})$. It can be seen that the horizontal velocity drops as the radial distance from the fault increases. This fast decay is due to the cylindrical aquifer geometry.

Figure 6 shows the temperature in the aquifer and the clay cap for two different mass flow rates and the indicated parameters. The results are obtained from the numerical integration of equations (62) and (63). The radial distance $\bar{r}$ is measured with respect to the length L'. Temperatures are seen to decrease with distance from the fracture zone at a given depth as a result of heat lost through the clay cap. Also, it is observed that higher mass flow rates produce higher temperatures, at a given $\bar{r}$-location. A well-defined thermal boundary layer exists near the fracture zone for $M = 5$. In contrast when $M = 0.5$ the aquifer is cooled significantly at depth even when $\bar{r} = 0.05$.

Isotherms in the aquifer for a high mass flow rate ($M = 5$) are shown in Fig. 7. It is observed that the horizontal temperature gradients decrease as the liquid spreads into the aquifer. A fast horizontal temperature gradient decay is seen in the region around the fracture zone due to the important cooling effect of the surface on the flow in this zone. It is noted that at a horizontal distance of 1.5 fracture-zone depths (aquifer portion) the system is nearly completely cooled to the background values. This may be compared to a horizontal cooling distance of about 10 L' found in the planar model. Once again, the difference is associated with the rapid decline

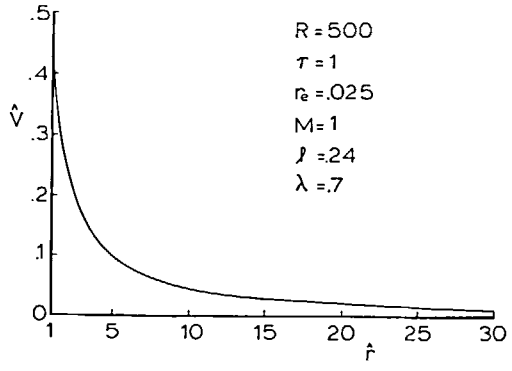

FIG. 5. Horizontal velocity $\hat{v}$ in the aquifer adjacent to the fracture zone as a function of radius $\hat{r}$ for $z = -0.5$.

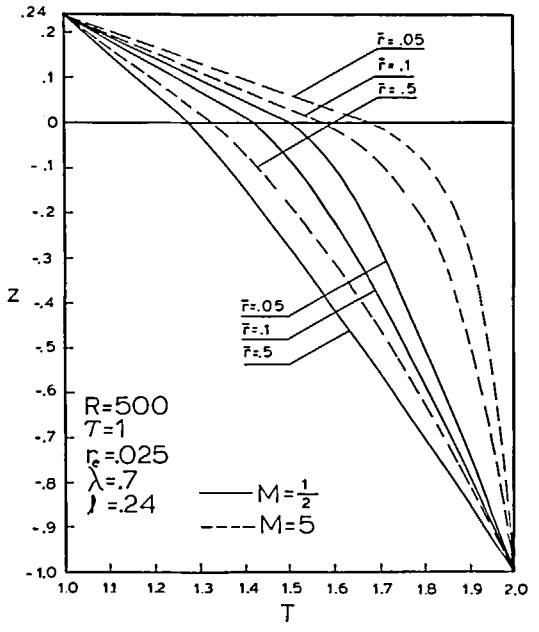

FIG. 6. Temperature in the clay cap and aquifer as a function of depth at several horizontal locations.

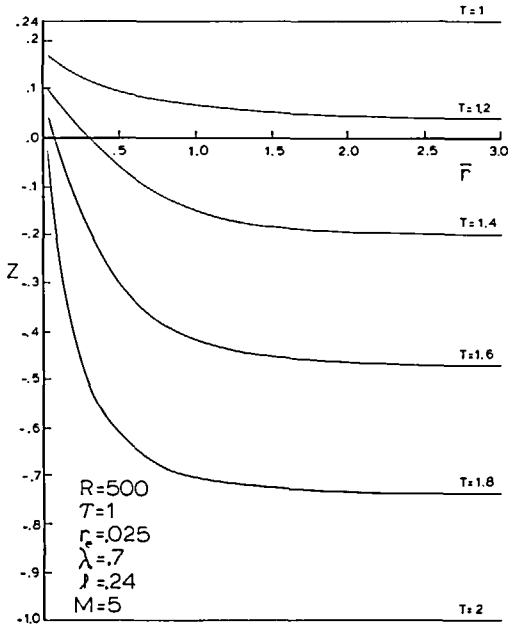

FIG. 7. Aquifer isotherm map in terms of the radial variable $\bar{r}$.

of the horizontal velocity in the axisymmetric geometry that leads to a relative enhancement of vertical conduction heat transfer.

Figures 8 and 9 show surface temperature gradients radially along the aquifer for different mass flow rates when $R = 500$ and $R = 1000$, respectively. The results are obtained from the numerical solution in the $\bar{r}$-region which can be used only for $\bar{r} \gtrsim 0.1$ because on this scale the fracture-zone radius is $\bar{r}_e = 0.025$. The transition from the surface temperature gradient value above the fracture zone of $-T_z^c = 4.17$, as found from equation (66), to the values above the aquifer could be obtained from the solution of equation (63) for $1 < \hat{r} \leqslant \infty$ and that for the equation for Region 1.

In general it is observed that an increase in the mass flux rate and/or an increase in the Rayleigh number enhances the heat flux above the aquifer. The transition from the common value of 4.17 above the fracture zone to the background value occurs more slowly for large M and/or R values.

Figure 10 shows the effect of fracture-zone radius variation on the surface temperature gradients for $M = 1$. When the non-dimensional mass flow rate (M) is kept constant, the effect produced by a larger cross section, in dimensional terms, is an increase in the dimensional mass rate. This increase produces an enhancement of the surface temperature gradients.

A comparison of Figs. 8, 9 and 10 permit one to assess the sensitivity of the surface heat flux to the system Rayleigh number R, to the mass input M and to the radius of the fracture zone r_e. For example, if we consider the results at $\bar{r} = 0.3$, we find a 17% enhancement of the heat flux at $R = 500$, $r_e = 0.025$ when M changes from 2 to 5. At $R = 1000$, the change is 31%. Alternatively, for $M = 2$, $r_e = 0.025$, there is a 10% increase in the flux when R increases from 500 to 1000. But when $M = 5$, the analogous variation is 21%. When $R = 500$, $M = 1$, quadrupling the fracture-zone area by increasing r_e from 0.025 to 0.05 causes a 61% increase in the heat flux. Similar variations can be found for any $\bar{r} = O(1)$. One may conclude that there is sufficient sensitivity in this quasi-analytical, parameterized study, to permit a selection of parameter values by comparing results with a specific set of surface heat flux measurements. One should be aware, however, that such a selection process will not be unique unless bore hole data is also available which would permit a comparison of temperature and pressure distribution with depth.

Figure 11 shows the surface temperature gradients along the aquifer for the planar configuration [3] and for the axisymmetric model for the indicated parameters. In the planar configuration r_e represents the semi-fault zone width. Comparing these two curves, it is apparent that faster cooling of the system occurs when an axisymmetric geometry is considered. This effect is principally due to the behaviour of the

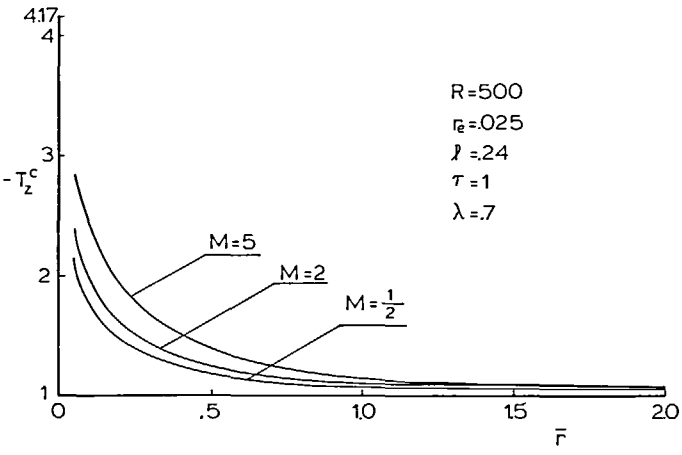

FIG. 8. Surface temperature gradient as a function of radial distance for several mass flow rates when $R = 500$.

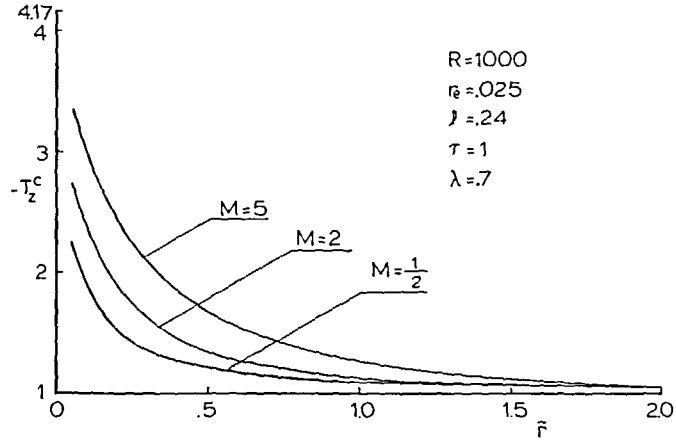

FIG. 9. Surface temperature gradient as a function of radial distance for several mass flow rates when $R = 1000$.

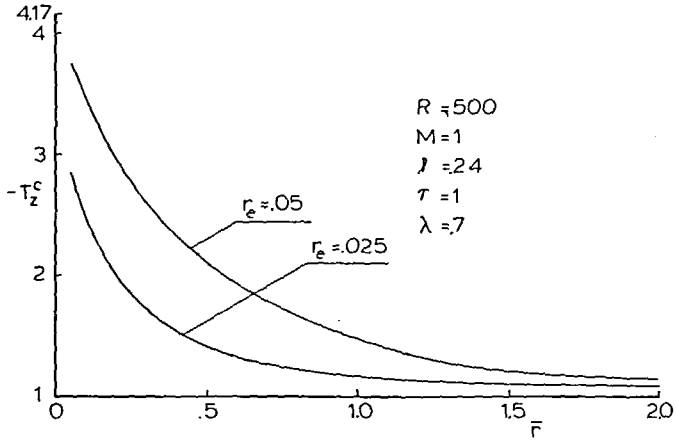

FIG. 10. Surface temperature gradient as a function of radial distance for two fracture zone radii when $R = 500$.

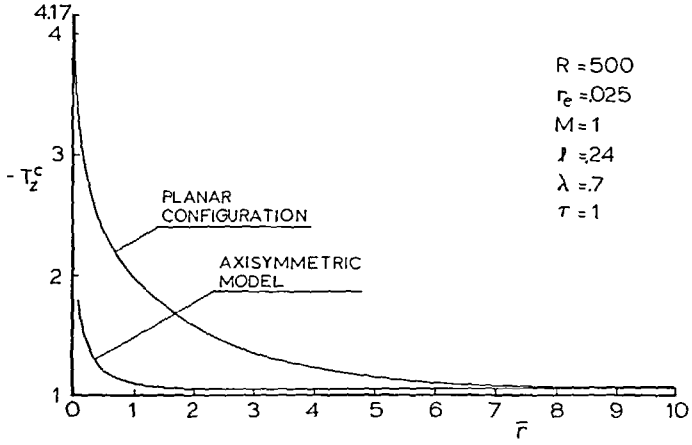

FIG. 11. A comparison of the surface temperature gradient variation with radial distance for the planar and axisymmetric models.

horizontal velocity in the aquifer. For the planar configuration the velocity depends only on the z-variable. In the axisymmetric geometry the velocity, in addition to its dependence on z, depends on the inverse of the radial distance $\bar{r}$ from the fracture zone, a dependence that leads to a diminution of its value as the radial distance from the fracture zone increases.

The Riney *et al.* model [4, 5, 26, 27] differs from that described here primarily because there is no explicit zone of high permeability in the reservoir in which extensive upflow can occur. In fact the vertical permeability k'_v in their model is never larger than 5×10^{-16} m^2 (0.5 md.). In comparison the horizontal value in most of the system is between $k'_h = 2 \times 10^{-14}$ m^2 (20 md.) and $k'_h = 9 \times 10^{-14}$ m^2 (90 md.). Hot liquid water is injected into the system in terms of a prescribed mass source located close to the reservoir–basement rock interface near the vertical axis. The low value of k'_v implies a characteristic vertical natural convection speed $q'_R = O(3.2 \times 10^{-8}$ cm s$^{-1})$ and an effective Rayleigh number $R = O(10^{-2})$ for their 2 km deep system. The latter parameter value implies that natural convection does not play a significant role in their model. Rather, large pressure gradients generated by processes beneath the reservoir must be present to drive the source fluid vertically upward through the low k'_v material into the shallower portions of the reservoir. Since the deeper portions of the system have relatively low horizontal permeability as well ($1–4 \times 10^{-10}$ cm^2), the radial spreading of the source fluid is minimized. The resulting forced convection jet of hot liquid begins to spread horizontally only in the shallow part of the reservoir where the larger k'_h values are found. For example, there is significant vertical upflow in the deep portion of the system out to 1500 m from the axis. The major horizontal outflow is confined to the upper 650 m of the reservoir. Heat loss from this convecting fluid to the surface enhances the purely vertical conductive flux out to a distance of about 8 km from the axis.

In the present model, the upflow region is confined to a radius of 86 m ($r_e = 0.025$) for $L' = 3.35$ km. The dimensional mass flux corresponding to $1 \leqslant M \leqslant 5$ for M'_R in equation (48) can be made to fit the Riney *et al.* values. Significant horizontal outflow occurs over the entire depth of the reservoir. The radial dropoff is described in Fig. 5. Figures 8–10 show that the convective distortion of the background conductive surface heat flux has basically gone 3–4 km ($\bar{r} \simeq 1$) from the axis.

Riney *et al.* [5] chose to exclude a local zone of high vertical permeability for two reasons. Given the bore hole data from the East Mesa field showing that the deep water in the system has a chemical composition rather distinct from that higher up they assumed that low permeability shales separated the deep highly saline water from the fresher water above. They then concluded that a distinct region of vertical permeability appeared to be incompatible with the observations. Secondly computations carried out with more significant vertical permeability in the aquifer produced physically unacceptable inverted temperature profiles resulting from extensive intrusion of cold recharge water at depth. These inversions were removed by reducing k'_v to the very small value mentioned earlier. As a result the temperature profiles are like those found in the present work where vertical motion in the aquifer is precluded.

In addition to the difference in assumed internal structure of the two models it should be recognized that somewhat different thermal boundary conditions are imposed. Riney *et al.* [4] assumed that the bottom boundary temperature varied from 196°C at the axis to 88°C at the far edge of the system. The present model employed a constant temperature of 200°C. A heat transfer coefficient model of heat loss at the top of the reservoir replaced the detailed conduction process through the cap to the surface in the Riney *et al.* study. The value of the coefficient is chosen so that the surface heat flux above the axis matches the field data. In comparison the full conduction equation is considered in the present model with a 25°C surface boundary condition and continuous temperature and heat flux through the cap–aquifer interface.

The cited differences between the models make qualitative comparisons difficult at best. Both models produce results which are least qualitatively compatible with real geothermal systems although the details of the plumbing are different. This suggests that at least for the surface heat flux signature, which Riney *et al.* [4, 5, 26, 27] used to validate their model, there is a certain insensitivity to conditions at depth.

8. CONCLUSIONS

A generic axisymmetric model for the charging of a geothermal reservoir has been developed. The system is assumed to have fairly simple material properties, an idealized geometry and thermal boundary conditions. Asymptotic methods, based on a large Rayleigh number approximation, are used to obtain solutions. It is shown that the physics of the heat transfer processes differ in distinct portions of the system. The region near the upflow zone is basically convection dominated while that far away is controlled primarily by vertical conduction. There is a convective–conductive balance in an intermediate location.

The cylindrical geometry is shown to have a direct effect on the surface heat flux distribution in comparison to that for a planar system. The inverse radial decline of the horizontal aquifer liquid speed reduces significantly the convective heat transport far from the upflow zone. As a result cylindrical systems are cooled to depth at a horizontal distance (from the axis of the upflow zone) which is only a small fraction of the system depth. In contrast a planar model is characterized by a deep region of hot isothermal flow to a distance of the magnitude of the system depth.

Acknowledgements—This work was supported by a grant from the U.S. Geological Survey Extramural Geothermal Program, 14-08-001-0628 and by a grant from the National

Science Foundation MEA-80-11730. We thank Professor J. Gary for providing assistance with numerical methods. The revised manuscript was prepared while the second author was a Senior Visiting Fellow in the School of Mathematics and Physics at the University of East Anglia, Norwich, U.K. The support of the Science and Engineering Research Council of the United Kingdom is gratefully acknowledged.

REFERENCES

1. K. P. Goyal and D. R. Kassoy, Fault zone controlled charging of a liquid dominated geothermal reservoir, *J. Geophys. Res.* **85**, 1867–1875 (1980).
2. K. P. Goyal, Heat and mass transfer in a saturated porous medium with applications to geothermal reservoirs, Ph.D. thesis, University of Colorado, Boulder, Colorado (1978).
3. K. P. Goyal and D. R. Kassoy, A plausible two-dimensional vertical model of the East Mesa geothermal field, California, U.S.A., *J. Geophys. Res.* **86**, 10719–10733 (1981).
4. T. D. Riney, J. W. Pritchett, L. F. Rice and S. K. Garg, Integrated model of the shallow and deep hydrothermal systems in the East Mesa area, Imperial Valley, California. Semi-annual Tech. Report No. 1, SSS-R-79-3995, Systems, Science and Software Inc., Box 1620, La Jolla, California, 92038 (1980).
5. T. D. Riney, J. W. Pritchett, L. F. Rice and S. K. Garg, Integrated model of the shallow and deep hydrothermal systems in the East Mesa area, Imperial Valley, California. Final Technical Report, SSS-R-80-4362, Systems, Science and Software Inc., Box 1620, La Jolla, California, 92038 (1980).
6. J. C. Troncoso, An axisymmetric mathematical model of a liquid-dominated hydrothermal system, M.S. thesis, University of Colorado, Boulder, Colorado (1981).
7. S. K. Garg and D. R. Kassoy, Convective heat and mass transfer in hydrothermal systems, in *Geothermal Systems, Principles and Case Histories* (edited by L. Rybach and L. J. P. Muffler), pp. 37–76. John Wiley, London (1981).
8. R. K. Hose and B. E. Taylor, Geothermal systems of northern Nevada U.S. Geological Survey, Open-file Rep. No. 74-271 (1974).
9. H. D. Murphy, Convective instabilities in vertical fractures and faults, *J. Geophys. Res.* **84**, 6121–6130 (1979).
10. R. P. Lowell, The onset of convection in a fault zone: effect of anisotropic permeability, *Trans. Geoth. Res. Coun.* **3**, 377–380 (1979).
11. M. L. Sorey, Numerical modeling of liquid geothermal systems, U.S. Geological Survey, Open-file Rep. No. 75-613 (1975).
12. M. Nathenson, T. C. Urban and W. H. Diment, Approximate solution for the temperature distribution caused by flow up a fault and its application to temperatures measured in a drill hole at raft river geothermal area, *Trans. Geoth. Res. Coun.* **3**, 477–480 (1979).
13. D. R. Kassoy and A. Zebib, Convection fluid dynamics in a model of a fault zone in the earth's crust, *J. Fluid Mech.* **88**, 769–792 (1978).
14. D. L. Turcotte, R. J. Ribando and K. E. Torrance, Numerical calculation of two-temperature thermal convection in a permeable layer with application to the Steamboat Springs thermal system, Nevada, in *The Earth's Crust* (edited by J. G. Heacock), Geophys. Monograph No. 20, pp. 722–736. American Geophysical Union, Washington, D.C. (1977).
15. J. Pritchett and S. Garg, Flow in an aquifer charged with hot water from a fault zone, *Pure Appl. Geophys.* **117**, 309–320 (1978).
16. D. S. Chapman, K. Kilty and C. Mase, Aspects of forced convection heat transfer in geothermal systems, Rep. 78-1701 a.6.4.1., University of Utah, Salt Lake City, Utah (1978).
17. T. C. Urban, W. H. Diment and M. Nathenson, East Mesa geothermal anomaly, Imperial Valley, California: significance of temperatures in a deep drill hole near thermal equilibrium, *Trans. Geoth. Res. Coun.* **2**, 79–82 (1978).
18. G. S. Bodvarsson, C. W. Miller and S. M. Benson, A simple model in fault-charged hydrothermal systems, LBL-12869 Revised, Lawrence Berkeley Lab., Berkeley, California (1981).
19. G. A. Waring (revised by R. R. Blankenship and R. Bentall), Thermal springs of the United States and other countries of the world—a summary, Prof. Pap. 492, U.S. Geological Survey (1965).
20. G. Bodvarsson, Physical characteristics of natural heat resources in Iceland, in *Proc. U.N. Conf. on New Sources of Energy*, Rome, Vol. 2, pp. 82–89 (1964).
21. D. L. Williams, R. P. Von Herzen, J. G. Sclater and R. N. Anderson, The Galapagos spreading center: Lithospheric cooling and hydrothermal circulation, *Geophys. J. R. Astr. Soc.* **38**, 587–608 (1974).
22. C. R. B. Lister, On the penetration of water into hot rock, *Geophys. J. R. Astr. Soc.* **39**, 465–509 (1974).
23. R. P. Lowell and C. T. Shyu, On the onset of convection in a water saturated porous box; effect of conducting walls, *Lett. Heat Mass Transfer* **5**, 371–378 (1978).
24. R. P. Lowell, Convection in narrow vertical fracture spaces, Final Technical Letter Report, Georgia Institute of Technology, Atlanta, Georgia (1980).
25. J. Howard, J. A. Apps. S. Benson, N. E. Goldstein, A. N. Graf, J. Haney, D. Jackson, S. Juprasert, E. Majer, D. McEdwards, T. V. McEvilly, T. N. Narasimhan, B. Schechter, R. Schroeder, R. Taylor, P. Van de Kamp and T. Wolery, Geothermal resource and reservoir investigations of U.S. Bureau of Reclamation leaseholds at East Mesa, Imperial Valley, CA, Rep. LBL-7094, Lawrence Berkeley Lab., Berkeley (1978)
26. T. D. Riney, J. W. Pritchett, L. F. Rice and S. K. Garg, A preliminary model of the East Mesa hydrothermal system (Proc. Fifth Stanford Geothermal Reservoir Engineering Workshop) Stanford Rept. SGP-TR-40, pp. 211–214 (1979).
27. T. D. Riney, J. W. Pritchett and L. F. Rice, Three dimensional model of East Mesa hydrothermal system, *Trans. Geoth. Res. Coun.* **4**, 377–380 (1980).
28. J. D. Cole, *Perturbation Methods in Applied Mathematics*, p. 72. Blaisdell, Waltham, Mass. (1968).

MODELE AXISYMETRIQUE POUR LE CHANGEMENT DU LIQUIDE D'UN RESERVOIR GEOTHERMIQUE

Résumé—On décrit les mécanismes de transfert massique et thermique dans un modèle de réservoir géothermique axisymétrique, dominé par le liquide. Le système est compose d'une région cylindrique verticale de roche fracturée entourée par une région aquifère annulaire, plus large. L'eau chaude liquide convectée dans la zone cylindrique centrale est forcée dans l'environnement aquifère. De la chaleur est perdue sur la surface froide lorsque le liquide s'écoule horizontalement (radialement) dans le volume aquifère. Une combinaison des techniques de couche limite et des méthodes numériques est utilisée pour obtenir des distributions de vitesse, de température et de pression dans le système et pour le flux thermique émanant de la surface de la roche. La portion profonde du volume aquifère axisymétrique est trouvée être refroidie plus vite que la partie équivalente d'un modèle plan.

EIN ACHSENSYMMETRISCHES MODELL FÜR DIE VERÄNDERUNGEN EINES DURCH FLÜSSIGKEITSSTRÖMUNGEN CHARAKTERISIERTEN GEOTHERMISCHEN RESERVOIRS

Zusammenfassung—Die Wärme- und Stofftransportvorgänge im Modell eines achsensymmetrischen, durch Flüssigkeitsströmungen charakterisierten geothermischen Reservoirs werden beschrieben. Das System besteht aus einem vertikalen zylindrischen Gebiet aus zertrümmertem Fels, umgeben von einem viel größeren, ringförmigen Aquifer. Heißes Wasser, das in die mittlere zylindrische Zone eindringt und aufsteigt, wird in das benachbarte Aquifer gedrückt. Wärme wird dabei an die kalte Oberfläche abgegeben, während die Flüssigkeit horizontal (radial) in das Aquifer strömt. Eine Kombination von Grenzschicht-Verfahren und numerischen Methoden wurde angewandt, um die Lösungen für Geschwindigkeit, Temperatur- und Druckverteilungen im System und für den Wärmestrom von der obersten Steinschicht an die Umgebung zu erhalten. Es zeigt sich, daß der untere Teil des achsensymmetrischen Aquifers sich schneller abkühlt als das entsprechende Gebiet eines ebenen Modells.

ОСЕСИММЕТРИЧНАЯ МОДЕЛЬ ЗАРЯДКИ ПОЧТИ ПОЛНОСТЬЮ ЗАПОЛНЕННОГО ЖИДКОСТЬЮ ГЕОТЕРМАЛЬНОГО РЕЗЕРВУАРА

Аннотация—Описываются процессы тепло-и массопереноса в модели геотермального резервуара, почти полностью заполненого жидкостью. Система состоит из вертикальной цилиндрической области, образованной растрескавшейся породой, которая окружена намного большей областью кольцевого водоносного слоя. Горячая вода, движущаяся внутрь и вверх по центральной цилиндрической зоне, проникает в соседний водоносный слой. При горизонтальном (радиальном) растекании жидкости в слое тепло поглощается холодной поверхностью. С помощью методов пограничного слоя и численных методов получены решения для распределений скорости, температуры и давления в системе и теплового потока с поверхности верхнего слоя породы. Найдено, что более глубокая часть осесимметричного водоносного слоя охлаждается быстрее, чем эквивалентная ее часть в плоской модели.